Synthesis and in vitro evaluation of pteridine analogues as monoamine oxidase B and nitric oxide synthase inhibitors

Louis H. A. Prins, Jacobus P. Petzer, Sarel F. Malan *

Pharmaceutical Chemistry, School of Pharmacy, North-West University, Private Bag X6001, Potchefstroom 2520, South Africa

ABSTRACT

Monoamine oxidase B (MAO-B) and nitric oxide synthase (NOS) have both been implicated in the pathology of neurodegenerative diseases. In an attempt to design dual-target-directed drugs that inhibit both these enzymes, a series of pteridine-2,4-dione analogues were synthesised. The compounds were found to be relatively weak NOS inhibitors but showed promising MAO-B activity with 6-amino-5-[(E)-3-(3-chloro-phenyl)-prop-2-en-(E)-ylideneamino]-1,3-dimethyl-1H-pyrimidine-2,4-dione and 6-[(E)-2-(3-chloro-phenyl)-vinyl]-1,3-dimethyl-1H-pteridine-2,4-dione inhibiting MAO-B with IC_{50} values of 0.602 and 0.314 μM, respectively. The pteridine-2,4-dione analogues thus show promise as scaffolds for the development of potent reversible MAO-B inhibitors and as observed in earlier studies, the most potent inhibitors were obtained with 3-chlorostyryl substitution.

© 2009 Elsevier Ltd. All rights reserved.

1. Introduction

Neurodegenerative disorders such as Parkinson's and Alzheimer's diseases, are affecting the lives of a growing number of people worldwide. These debilitating conditions lead to a general decrease in quality of life and the need for therapeutics to effectively prevent and treat these conditions are of increasing importance.[1]

It has become evident that neurodegenerative diseases are not the result of a single cause but that the processes involved are of a multifactorial nature. It is hypothesised that genetic, environmental and endogenous factors may be involved in neurodegenerative diseases such as Alzheimer's disease, Parkinson's disease, Huntington's disease and amyotrophic lateral sclerosis. A series of general pathways has been identified that may be involved in different pathogenic cascades and includes protein misfolding and aggregation, oxidative stress and free radical formation, metal dyshomeostasis, mitochondrial dysfunction and phosphorylation impairment. All of the above seem to occur simultaneously, leading to the demise of key neuronal cells.[2]

Keeping this in mind, the paradigm of targeting a single disease factor may not be an effective treatment strategy for neurodegenerative diseases. The polypharmaceutical approach, wherein several drugs that act independently on different etiological targets

of a disease are combined, has been used as a means of multiple targeting in the clinical setting. However, this strategy of combining several drug molecules results in several challenges, such as a combined or even multiplied toxicity and side-effect profile and the occurrence of unforeseen drug–drug interactions.[3] For these reasons the design of single drug molecules that act on two or more specific etiological targets of a particular disease may be of value. The advantages associated with this strategy includes a lower likelihood of encountering unwanted side-effects and the possibility to 'design out' any side-effects when only using one drug, as opposed to using two or more drugs.[1]

One target for the treatment of neurodegenerative diseases is the enzyme monoamine oxidase B (MAO-B). It is the predominant isoform of MAO found in human brain[4] where it is implicated in age-related neurodegenerative diseases such as Parkinson's disease and Alzheimer's disease. It has been demonstrated that brain MAO-B activity, but not MAO-A activity, increases with aging,[5] and since MAO-B appears to be located in glial cells this may be due to gliosis associated with aging. MAO-B plays a dual role in the pathophysiology of Parkinson's disease since it is a major dopamine metabolising enzyme and is also implicated in the formation of reactive oxygen species and other neurotoxic species.[6] MAO-B has also been implicated in the pathophysiology of Alzheimer's disease since increased MAO-B levels have been observed in plaque-associated astrocytes in the brains of Alzheimer's disease patients.[7] This increase in MAO-B activity may result in an elevation in hydroxyl radicals (·OH), which has been correlated with amyloid-β (Aβ) plaque formation. Hence, the therapeutic potential of selective reversible MAO-B inhibitors does not rely solely on

* Corresponding author at present address: School of Pharmacy, University of the Western Cape, Private Bag X17, Bellville 7535, South Africa. Tel.: +27 21 9593190; fax: +27 21 9591588.
E-mail address: sfmalan@uwc.ac.za (S.F. Malan).

their ability to increase the biological half-life of dopamine but also on their ability to reduce the levels of MAO-B generated reactive oxygen species in the brain and their potential ability to inhibit Aβ plaque formation.

Another enzyme implicated in the neurodegenerative process is nitric oxide synthase (NOS). Nitric oxide (NO) is known to be an important cell signalling agent that regulates an array of physiological functions. These include blood pressure by regulation of smooth muscle relaxation,[8] platelet aggregation by acting as an antithrombotic agent,[9] antitumor, antibacterial, and antiviral action of macrophages,[10] brain development, learning and memory,[11] and it is also the neuronal mediator of penile erection.[12] However, since NO is a free radical, overproduction thereof may result in deleterious effects ranging from septic shock and pain[13] to ischaemia[14] and it may also be involved in neurodegenerative processes[15] associated with Parkinson's and Alzheimer's diseases.[16] The harmful effects caused by an overproduction of NO are thought to be mediated by peroxynitrite (ONOO$^-$), the product obtained when NO and the superoxide radical (O$_2$·$^-$) react. ONOO$^-$ causes injury to the mitochondrial electron transport chain resulting in damage and eventual death of neurons. Evidence that NO and ONOO$^-$ are neurotoxic is provided in the ability of superoxide dismutase to protect cortical cultures from both glutamate and NO donors. Removal of nNOS containing neurons from culture or elimination of nNOS through transgenic technology, results in a culture that is resistant to NMDA neurotoxicity indicating that nNOS neurons are the source of neurotoxic NO.[16,17]

Several 8-substituted caffeinyl derivatives have been reported to be moderate to potent reversible inhibitors of MAO-B.[18,19] For example, the caffeine analogue (E)-8-(3-chlorostyryl)-caffeine (CSC) (1, Fig. 1), is an exceptionally potent MAO-B inhibitor, with enzyme-inhibitor dissociation constants (K_i values) of 100 nano molar (nM) for mouse brain mitochondrial MAO-B[20] and 128 nM for baboon liver mitochondrial MAO-B.[21] Pteridine-2,4-dione (2) bear structural resemblance to caffeine (3) and was therefore of interest in the design of novel reversible MAO-B inhibitors, possibly with comparable activity to the caffeinyl derivatives. The synthesis of pteridine-2,4-diones conjugated to styryl and other moieties were thus pursued, and the resulting compounds were evaluated as MAO-B inhibitors.

Pteridine-2,4-dione is also structurally similar to the essential NOS cofactor, tetrahydrobiopterin (BH$_4$) (4) and certain pterin analogues (5) have been developed to target this binding site.[22,23] Because of this structural relationship with BH$_4$, pteridine derivatives have been described as NOS inhibitors. Since BH$_4$ exhibits lower affinity and selectivity for other pterin dependent enzymes, this approach appears to be promising.[24] In a series of BH$_4$ analogues the 4-amino derivative, 5,6,7,8-tetrahydro-6-(D-threo-1,2-dihydroxypropyl)pterin (6), was reported to be a potent inhibitor of recombinant rat brain NOS in vitro (K_i = 13 nM) as well as in vivo.[25] Also of interest is the 6-phenyl derivative (7) which inhibits NOS with an IC$_{50}$ value of 6 μM. Based on the NOS inhibition activity of pterin analogues, the structurally similar pteridine-2,4-dione analogues prepared in the present study were also evaluated as NOS inhibitors. Compounds that inhibit both MAO-B and NOS may find enhanced application in the treatment of neurodegenerative disorders.
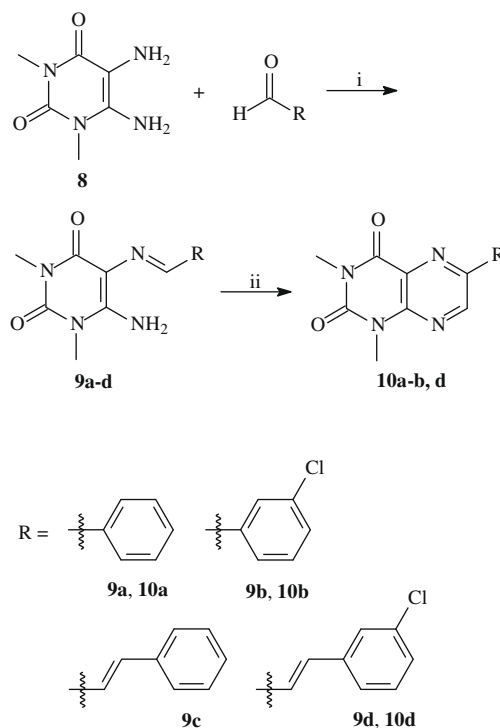
2. Results

2.1. Synthesis of pteridine-2,4-dione analogues

The target pteridine-2,4-dione derivatives were synthesised according to the literature procedure (Scheme 1).[26] The key
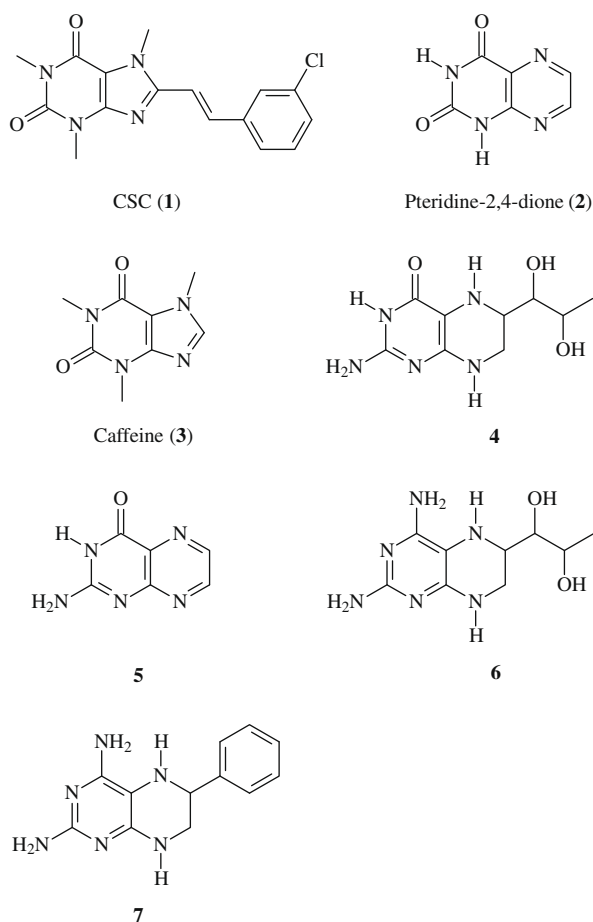
Figure 1. The structures of CSC (1), pteridine-2,4-dione (2), caffeine (3) and selected pterin analogues.

Scheme 1. Synthetic pathway to pteridine-2,4-dione (10) and pyrimidine (9) analogues. Reagents and conditions: (i) EtOH, reflux, 4 h; (ii) CH(OCH$_2$CH$_3$)$_3$, DMF, reflux, 10 h.

starting material, 1,3-dimethyl-5,6-diaminouracil (**8**), was reacted with the appropriate aldehyde to yield the pyrimidines **9a–d**. The pyrimidines were cyclised by the addition of triethyl orthoformate under reflux, to obtain the final pteridine-2,4-diones **10a–b, d**.[26] Cyclisation of **9c** using this procedure was not successful and the corresponding pteridine-2,4-dione could not be obtained. The structures of the newly synthesised compounds were confirmed by ^{1}H NMR, ^{13}C NMR, IR, MS and elemental analyses.

2.2. MAO-B inhibition

It has previously been shown that baboon liver tissue is devoid of MAO-A activity while exhibiting a high degree of MAO-B catalytic activity.[27] The interaction of reversible inhibitors with baboon liver MAO-B also appears to be similar to human liver MAO-B.[19] Recent results from our laboratory (unpublished data) have also indicated that a variety of structurally unrelated compounds inhibit membrane bound baboon liver and recombinant human MAO-B with similar potencies. Mitochondrial fractions obtained from baboon liver were thus used to determine the extent by which the pteridine-2,4-dione analogues (**10a–b, d**) and the pyrimidines (**9a–d**) inhibit this enzyme.
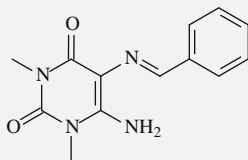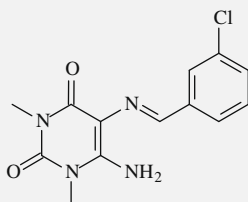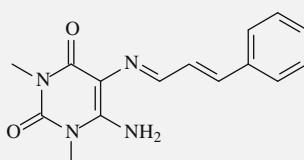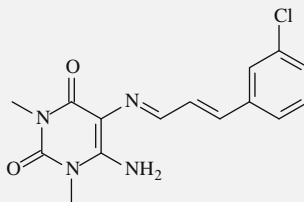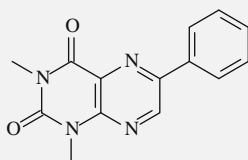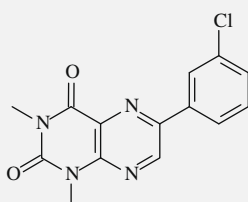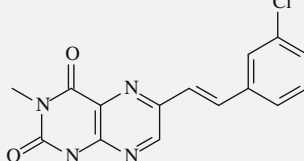
IC_{50} values (concentration of the inhibitor that inhibits 50% of the enzyme activity) for the test compounds were determined by measuring the extent by which different concentrations thereof slowed the rate of α-carbon oxidation of 1-methyl-4-(1-methyl-pyrrol-2-yl)-1,2,3,6-tetrahydropyridine (MMTP) to the corresponding dihydropyridinium metabolite, MMDP$^+$ (Fig. 2). The production of MMDP$^+$ was measured spectrophotometrically at a wavelength of 420 nm, at which neither the substrate nor the test compounds absorb UV light.

The results of the MAO-B activity measurements indicate that **10d** is the most potent MAO-B inhibitor of the analogues examined in this study, with an IC_{50} value of 0.314 μM (Table 1). The second most potent inhibitor was pyrimidine **9d** with with an IC_{50} value of 0.602 μM. It is noteworthy that **10d** and **9d** are structurally closely related to CSC (**1**), a known MAO-B inhibitor. Using the Cheng–Prusoff equation[28] the K_i values (enzyme–inhibitor dissociation constants) for the inhibition of MAO-B by **10d** and **9d** were calculated to be 181 and 348 nM, respectively, indicating that **10d** is only slightly less potent than CSC (K_i = 128 nM)[21] as a MAO-B inhibitor.
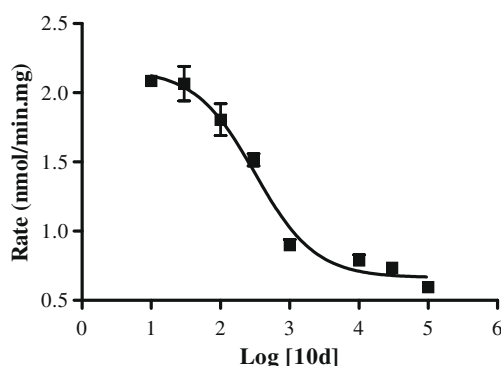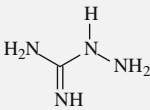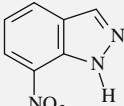
Figure 2. The sigmoidal dose–response curve of the initial rates of oxidation of MMTP versus the logarithm of concentration of inhibitor **10d** (expressed in nM). The concentration of the baboon liver mitochondrial preparation was 0.15 mg protein/mL. The rates are expressed as nmol MPDP$^+$ formed/mg protein/min and the concentration of MMTP used was 50 μM. The determinations were carried out in duplicate and the values are expressed as mean ± SEM.

Table 1
MAO-B and NOS inhibition by pteridine-2,4-dione (**10**) and pyrimidine (**9**) analogues

Compound	MAO-B inhibition		NOS inhibition
	IC_{50} (μM)	K_i (μM)[c]	IC_{50} (μM)
9a	Not determined[a]	Not determined[a]	466.9
9b	7.033	4.060	6968
9c	12.052	6.958	Not determined[d]
9d	0.602	0.348	577.2
10a	Not determined[b]	Not determined[b]	443.3
10b	4.889	2.823	Not determined[d]
10d	0.314	0.181	1057

Table 1 (continued)

Compound	MAO-B inhibition		NOS inhibition
	IC_{50} (μM)	K_i (μM)[c]	IC_{50} (μM)
AG	–	–	19.41[e]
7-NI	–	–	0.111[e]

[a] At the limit of solubility (30 μM) 17.8% of the MAO-B activity was inhibited.

[b] At the limit of solubility (100 μM) 12.2% of the MAO-B activity was inhibited.

[c] The experimentally determined IC_{50} values were used to calculate the K_i values according to the equation by Cheng and Prusoff: $K_i = IC_{50}/(1 + [S]/K_m)$ with $[S] = 50$ μM and K_m (MMTP) = 68.3 ± 1.60 μM.[28]

[d] Values could not be calculated as these compounds absorb UV light within the assay detection range (390–430 nm).

[e] Values obtained from Joubert et al. (2008).[31]

2.3. NOS inhibition

In order to determine the NOS inhibition potencies of the pteridine-2,4-dione (**10a–b, d**) and pyrimidine (**9a–d**) analogues, the oxyhaemoglobin (Hb) assay[29] was used. This assay is based on the measurement of the conversion of oxyHb to metHb by NO (Fig. 3). Rat brain homogenate was used as NOS enzyme source since it has been shown to have high constitutive NOS activity.[30] A disadvantage of brain homogenate as enzyme source is that isoform selectivity is unaccounted for since the crude rat brain extract contains several NOS isoforms. For the purpose of screening potential NOS inhibitors for central NOS inhibition activity, this enzyme source was deemed appropriate.

Comparing the obtained IC_{50} values for the pteridine-2,4-diones (**10a–b, d**) and pyrimidines (**9a–d**) to those of two known NOS inhibitors, 7-nitroindazole (7-NI; $IC_{50} = 0.111$ μM) and aminoguanidine (AG; $IC_{50} = 19.41$ μM), reveals that none of the test compounds are promising as potential NOS inhibitors (Table 1). The most potent inhibitors were **10a** ($IC_{50} = 443.3$ μM) and **9a** ($IC_{50} = 466.9$ μM), which are approximately 23-fold less potent than AG. IC_{50} values could not be calculated for compounds **9c** and **10b** since these compounds absorb UV light in the detection range (390–430 nm) of the assay.
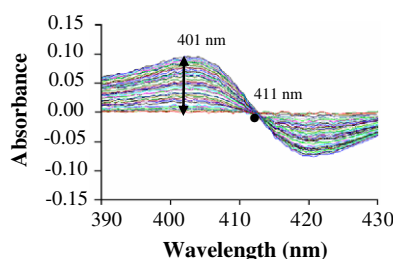

Figure 3. UV–vis scans of incubations containing rat brain homogenate, oxyHb, NADPH and L-arginine. The increase in absorbance intensity at a wavelength of 401 nm is indicative of metHb production as a result of NO formation by NOS present in the homogenate fraction.

2.4. Molecular modelling study

In an attempt to clarify the relationships between the observed MAO-B inhibition potencies and the structures of the inhibitors examined here, molecular docking studies with the active pyrimidine (**9b–d**) and pteridine (**10b, d**) analogues were performed. CSC (**1**) and safinamide were also included in the docking study. The crystallographic structure of recombinant human MAO-B in complex with the reversible inhibitor safinamide (PDB code: 2V5Z)[32] was selected for the docking studies. Since safinamide spans both the entrance and substrate cavities of the enzyme active site, the side chain of the gating residue, Ile-199, is rotated out of its normal conformation to allow for the fusion of the two cavities and the accommodation of larger structures such as those examined in the present study.[33] To evaluate the accuracy of the docking procedure, the co-crystallised ligand was redocked within the active site using the LigandFit application within Discovery Studio® 1.7. This procedure was repeated three times and the best ranked solution of safinamide in each instance exhibited a RMSD of 1.73 Å from the co-crystallised ligand (Fig. 4). In general, RMSD values smaller than 2.0 Å indicate that the docking protocol is capable of accurately predicting the binding orientation of the co-crystallised ligand.[34] This protocol was thus deemed to be suitable for docking of the inhibitors into the active site model of MAO-B.

The best ranked docking solutions of the pyrimidine (**9b–d**) and pteridine (**10b, d**) analogues examined here show that all inhibitors span both the entrance and substrate cavities of the enzyme. As shown for example with **9d** (Fig. 5) and **10d** (Fig. 6), the pyrimidine-2,4-dione rings of **9b–d** and the pteridine-2,4-dione rings of **10b, d** are located within the substrate cavity nearer to the FAD cofactor. The phenyl (**9b, 10b**) and styryl (**9c–d, 10d**) side chains extend towards the entrance cavity. These binding modes are expected since the polar regions in the substrate cavity would better
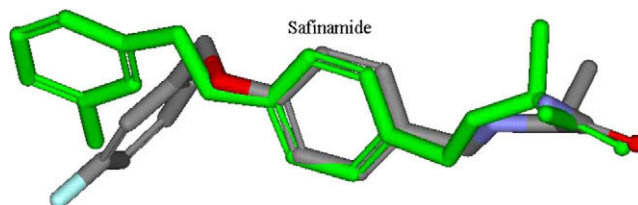
Figure 4. RMSD overlay of the best ranked solutions of safinamide on the original co-crystallised ligand, displayed in bright green.
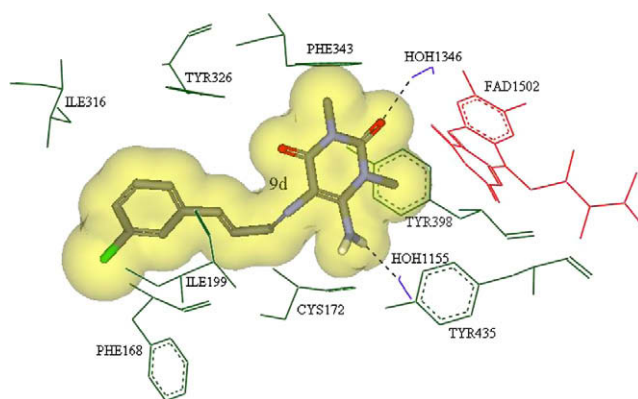
Figure 5. Putative binding mode of **9d** to the human MAO-B active site. Hydrogens are hidden, except those involved in hydrogen bonds, and selected amino acid residues are displayed in dark green. The FAD cofactor is indicated in red, interacting water molecules in blue and hydrogen bonds in black. The Van der Waals volume of **9d** is displayed as a transparent yellow surface.
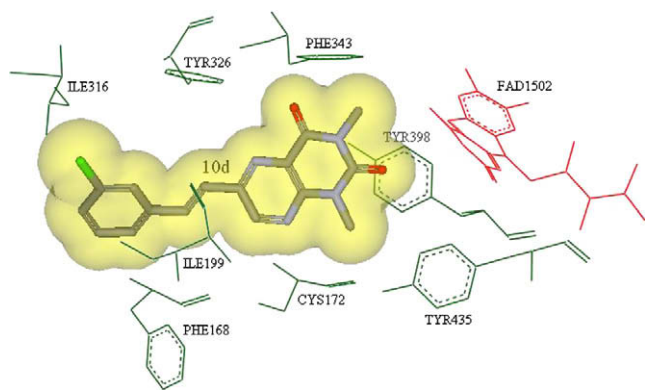
Figure 6. Putative binding mode of **10d** to the human MAO-B active site. Hydrogens are hidden, except those involved in hydrogen bonds, and selected amino acid residues are displayed in dark green. The FAD cofactor is indicated in red, interacting water molecules in blue and hydrogen bonds in black. The Van der Waals volume of **10d** is displayed as a transparent yellow surface.

Figure 8. Putative binding mode of CSC to the human MAO-B active site. Hydrogens are hidden, except those involved in hydrogen bonds, and selected amino acid residues are displayed in dark green. The FAD cofactor is indicated in red, interacting water molecules in blue and hydrogen bonds in black. The Van der Waals volume of CSC is displayed as a transparent yellow surface.

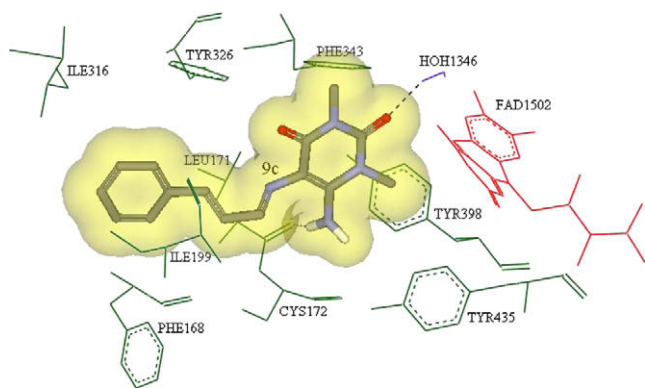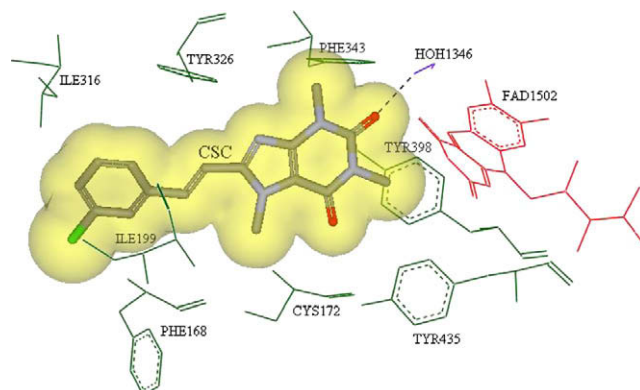accommodate the pyrimidine and pteridine rings while the phenyl and styryl moieties would be better stabilised within the hydrophobic entrance cavity. In addition, hydrogen bonding between the carbonyl oxygens of the pyrimidine and pteridine rings and integral water molecules within the substrate cavity would further promote these binding orientations.

For structures **9b–d** the possibility of hydrogen bond formation with the amino functional group on C6 of the pyrimidine ring also exists as demonstrated in Figure 7. CSC adopts a similar binding mode to those observed for the pyrimidine (**9b–d**) and pteridine (**10b, d**) analogues and the caffeine ring of CSC is located in the substrate cavity of the MAO-B active site model while the styryl side chain extends into the entrance cavity (Fig. 8). As observed for the pyrimidine and pteridine analogues, the caffeine carbonyl oxygens can also act as potential hydrogen bond acceptors within the substrate cavity.

The log IC$_{50}$ values of the pyrimidine (**9c–d**) and pteridine (**10d**) analogues and of CSC correlated with the DockScore value with a correlation coefficient (r^2 value) of 0.97 (Table 2). Although it is extremely difficult to accurately rank compounds based on their binding affinity in a docking study, this observation may serve as additional evidence that this docking protocol is effective for examining the molecular interactions between the inhibitors studied here and the active site of MAO-B. This docking protocol also appears to have predictive value and may in the future be developed as a predictive model for MAO-B inhibition.

Table 2
Comparison of calculated affinities (DockScore values) of compounds **9c**, **9d**, **10d** and CSC with experimental MAO-B inhibitory activities (log IC$_{50}$ values)

Ligand	DockScore	log IC$_{50}$ (µM)
CSC	60.171	−0.836[a]
10d	59.898	−0.503
9d	57.842	−0.220
9c	54.249	1.081

[a] Value obtained from the literature.[35]

3. Discussion

The current study has identified pteridine-2,4-diones as promising novel inhibitors of MAO-B. Analogue **10d** which is substituted with a 3-chlorostyryl functional group at C6 of the pteridine-2,4-dione ring was found to be the most potent inhibitor with an IC$_{50}$ value of 0.314 µM. This inhibition potency is comparable to that of CSC, a potent reversible MAO-B inhibitor.[20,21,35] Interestingly, the pteridine-2,4-diones were found to be more potent MAO-B inhibitors than their corresponding pyrimidine precursors. For example pyrimidine **9d**, the precursor of **10d,** has an IC$_{50}$ value of 0.602 µM compared to the 0.314 µM of **10d**. The same trend is observed for pteridine-2,4-dione **10b**, which is more potent than pyrimidine **9b**. A possible reason for this observation is that the amine functional group at C6 of the pyrimidine ring might be protonated at physiological pH. This may hinder access to the active site or prevent effective binding within the site.

The current study also shows that styryl substitution at C6 of the pteridine-2,4-dione results in better MAO-B inhibitors than phenyl substitution. For example **10d** was approximately 16-fold more potent as a MAO-B inhibitor than was **10b**. Chlorine substitution at C3 of the styryl ring was again found to be important for binding to the active site of MAO-B[19,20] and throughout both the pyrimidine and pteridine series, the chlorine substituted compounds exhibited higher activity as MAO-B inhibitors. This concurs with the reported findings that CSC is approximately 22-fold more potent than the corresponding unsubstituted (E)-8-styrylcaffeines.[21] This data suggests that the inhibitors examined here have a similar binding mode as CSC. In general, substitution of the styryl ring appears to improve the binding interactions within the entrance cavity.

As has been the case in numerous other enzymatic studies, the limited solubility of the test compounds in this study restricted the full exploration of their biological profile. In the MAO-B assay

Figure 7. Putative binding mode of **9c** to the human MAO-B active site. Hydrogens are hidden, except those involved in hydrogen bonds, and selected amino acid residues are displayed in dark green. The FAD cofactor is indicated in red, interacting water molecules in blue and hydrogen bonds in black. The Van der Waals volume of **9c** is displayed as a transparent yellow surface.

for example, compound **10a** and its pyrimidine precursor **9a** were insoluble in the buffer medium at 100 and 30 μM, respectively. Another factor specifically relating to the NOS oxyHb assay, which hindered biological evaluation, was the UV absorption properties of the test inhibitors. Compounds **9c** and **10b** were both shown to absorb UV light in the assay detection range stretching from 390 to 430 nm. As a result, NOS inhibition data could not be calculated for either of these compounds. As none of the pteridine analogues showed promise as NOS inhibitors, neither the obtained results nor the assay procedure were optimised any further.

4. Conclusion

Although multifunctional drugs are a promising strategy for the treatment of neurodegenerative diseases,[36,37,1] designing drugs that act at multiple targets remains a challenge. Designing pteridine analogues to target the BH$_4$ binding site of NOS was not successful in this study and it is hypothesised that the styryl phenyl may be sterically hindering binding of the test compounds to NOS.

Comparing the calculated MAO-B K_i values for the synthesised pteridines (Table 1) with those experimentally determined for a series of benzimidazoles,[38] reveals that pteridines may be better scaffolds for MAO-B inhibition than benzimidazoles and in general exhibit MAO-B inhibition only slightly less potent than that observed with the corresponding caffeine structures. These compounds thus show potential for the design of potent reversible MAO-B inhibitors and might, with optimisation, be attractive alternatives to the caffeine analogues.

5. Experimental

Caution: MMTP is a structural analogue of the nigrostriatal neurotoxin, 1-methyl-4-phenyl-1,2,3,6-tetrahydropyridine (MPTP) and it should be handled using disposable latex gloves and protective eyewear. Procedures for the safe handling of neurotoxic compounds were followed as described previously.[39]

5.1. Materials and instrumentation

All chemicals and reagents were purchased from commercial sources and solvents were dried using standard methods. 1,3-Dimethyl-5,6-diaminouracil (**8**),[40] *trans*-3-chloro-cinnamaldehyde[41] and the oxalate salt of MMTP[42] were prepared according to previously reported methods. Because of chemical instability, **8** was used within 24 h of preparation. Thin-layer chromatography was performed on 0.20 mm thick aluminium silica gel sheets (Alugram® SIL G/UV$_{254}$, Kieselgel 60, Macherey-Nagel® Düren, Germany) with an appropriate mobile phase and visualisation was achieved using UV light (254 and 366 nm) and iodine vapour. All melting points (mp) were obtained using a Stuart® SMP10 melting point apparatus and are uncorrected. ^{1}H and ^{13}C NMR spectra were recorded using a Bruker® Avance III 600 spectrometer at a frequency of 600 and 150 MHz, respectively. Chemical shifts are expressed in parts per million (δ) relative to the signal from tetramethylsilane (Me$_4$Si), added to an appropriate deuterated solvent (CDCl$_3$ or DMSO-d_6). Spin multiplicities are given as s (singlet), d (doublet), dd (doublet of doublets) and m (multiplet). Mass spectra were obtained by direct insertion electron impact ionisation mass spectrometry (EI-MS) using an analytical VG 7070E mass spectrometer. IR spectra were recorded in KBr on a Nicolet® Nexus™ 470-FT IR spectrometer over the range 400–4000 cm^{-1} employing the diffuse reflectance method. Elemental analyses were done using a Perkin–Elmer® 2400 Series II CHNS elemental analyser with argon gas as carrier.

5.2. Synthesis

General procedure for the synthesis of pyrimidines **9a–d**: 1,3-Dimethyl-5,6-diaminouracil (17.6 mmol) was suspended in 10 mL ethanol (anhydrous). The appropriate aldehyde (20.6 mmol) was dissolved in 5 mL ethanol (anhydrous) and added to the above suspension. After heating the mixture under reflux for 4 h it was allowed to cool to room temperature. The reaction was cooled on an ice bath for 30 min and the precipitate was collected by filtration and washed with ethanol. Recrystallisation from DMF/H$_2$O gave the pure intermediary compounds (**9a–d**) in excellent yield.

General procedure for the synthesis of pteridine-2,4-dione analogues **10a–d**: The appropriate pyrimidine compound (**9a–b, d**, 8.5 mmol) was dissolved in 10 mL *N,N′*-dimethylformamide at ambient temperature and triethyl orthoformate (43 mmol) was added. The solution was refluxed for 10 h and then allowed to cool to room temperature. The reaction was incubated on an ice bath for 30 min and the resulting precipitate was collected by filtration. The pteridine-2,4-diones were recrystallised from *N,N′*-dimethylformamide (**10a, 10b**) or acetone (**10d**).

5.2.1. 6-Amino-1,3-dimethyl-5-{[1-phenylmeth-(*E*)-ylidene]-amino}-1*H*-pyrimidine-2,4-dione (9a)

Compound **9a** was prepared from 1,3-dimethyl-5,6-diaminouracil (**8**) and benzaldehyde in a yield of 59.2%. C$_{13}$H$_{14}$N$_4$O$_2$; mp: 225 °C (DMF/H$_2$O). The measured melting point was in accordance with the literature value (225 °C).[26]

5.2.2. 6-Amino-5-{[1-(3-chlorophenyl)-meth-(*E*)-ylidene]-amino}-1,3-dimethyl-1*H*-pyrimidine-2,4-dione (9b)

Compound **9b** was prepared from 1,3-dimethyl-5,6-diaminouracil (**8**) and 3-chloro-benzaldehyde in a yield of 78.6%. C$_{13}$H$_{13}$ClN$_4$O$_2$; mp: 253 °C (DMF/H$_2$O); ^{1}H NMR (600 MHz, DMSO-d_6) δ_H: 9.71–9.67 (s, 1H), 8.07–7.71 (m, 2H), 7.46–7.33 (m, 4H), 3.42–3.37 (s, 3H), 3.19–3.14 (s, 3H); ^{13}C NMR (150 MHz, DMSO-d_6) δ_C: 157.70 (C), 154.20 (C), 150.00 (CH), 148.00 (C), 141.20 (C), 134.10 (C), 130.60 (CH), 129.00 (CH), 126.90 (CH), 126.20 (CH), 99.10 (C), 30.90 (CH$_3$), 27.50 (CH$_3$); MS (EI, 70 eV) *m/z*: 292 (M$^+$); IR (KBr) ν_{max}: 3414, 3297, 3081, 1690, 1551, 1593, 1518, 1449, 1263, 1226, 1207, 1067, 876, 789, 760, 748, 711 cm^{-1}; Anal. Calcd for C$_{13}$H$_{13}$ClN$_4$O$_2$: C, 53.34; H, 4.48; N, 19.14. Found: C, 54.20; H, 4.30; N, 19.40.

5.2.3. 6-Amino-1,3-dimethyl-5-[(*E*)-3-phenyl-prop-2-en-(*E*)-ylideneamino]-1*H*-pyrimidine-2,4-dione (9c)

Compound **9c** was prepared from 1,3-dimethyl-5,6-diaminouracil (**8**) and *trans*-cinnamaldehyde in a yield of 76.1%. C$_{15}$H$_{16}$N$_4$O$_2$; mp: 235 °C (DMF/H$_2$O); ^{1}H NMR (600 MHz, DMSO-d_6) δ_H: 9.48–9.45 (d, 1H, *J* = 8.21 Hz), 7.55–7.52 (d, 2H, *J* = 8.62 Hz), 7.39–7.25 (m, 5H), 7.00–6.97 (d, 2H, *J* = 8.00 Hz), 3.36 (s, 3H), 3.15 (s, 3H); ^{13}C NMR (150 MHz, DMSO-d_6) δ_C: 156.81 (C), 153.26 (C), 151.32 (CH), 149.63 (2 × C), 136.53 (CH), 131.62 (CH), 128.73 (2 × CH), 128.12 (2 × CH), 126.59 (CH), 99.39 (C), 30.21 (CH$_3$), 26.99 (CH$_3$); MS (EI, 70 eV) *m/z*: 285 (M$^+$); IR (KBr) ν_{max}: 3498, 3374, 3061, 3032, 2996, 1680, 1608, 1585, 1518, 1448, 1226, 1162, 1068, 973, 916, 840, 766, 747, 694 cm^{-1}; Anal. Calcd for C$_{15}$H$_{16}$N$_4$O$_2$: C, 63.37; H, 5.67; N, 19.71. Found: C, 62.60; H, 5.60; N, 18.80.

5.2.4. 6-Amino-5-[(*E*)-3-(3-chloro-phenyl)-prop-2-en-(*E*)-ylideneamino]-1,3-dimethyl-1*H*-pyrimidine-2,4-dione (9d)

Compound **9d** was prepared from 1,3-dimethyl-5,6-diaminouracil (**8**) and *trans*-3-chlorocinnamaldehyde in a yield of 59.9%. C$_{15}$H$_{15}$ClN$_4$O$_2$; mp: 222 °C (DMF/H$_2$O); ^{1}H NMR (600 MHz, DMSO-d_6) δ_H: 9.44–9.42 (d, 1H, *J* = 8.76 Hz), 7.61–7.49 (m, 2H), 7.42–7.28 (m, 4H), 7.10–7.02 (dd, 1H, *J* = 8.79, 16.13 Hz), 6.98–

6.92 (d, 1H, J = 16.18 Hz), 3.40–3.36 (s, 3H), 3.19–3.14 (s, 3H); ^{13}C NMR (150 MHz, DMSO-d_6) δ_C: 157.20 (C), 154.00 (C), 151.10 (CH), 150.09 (C), 139.50 (C), 135.00 (C), 134.10 (CH), 133.70 (CH), 131.10 (CH), 128.10 (CH), 125.75 (CH), 100.00 (CH), 30.90 (CH$_3$), 27.80 (CH$_3$); MS (EI, 70 eV) m/z: 318 (M$^+$); IR (KBr) ν_{max}: 3411, 3323, 3125, 3054, 3029, 1684, 1611, 1559, 1509, 1438, 1280, 1218, 1165, 1068, 898, 871, 791, 749, 702 cm^{-1}; Anal. Calcd for C$_{15}$H$_{15}$ClN$_4$O$_2$: C, 56.52; H, 4.74; N, 17.58. Found: C, 56.20; H, 4.40; N, 17.90.

5.2.5. 1,3-Dimethyl-6-phenyl-1*H*-pteridine-2,4-dione (10a)

Compound **10a** was prepared from 6-amino-1,3-dimethyl-5-{[1-phenylmeth-(*E*)-ylidene]-amino}-1*H*-pyrimidine-2,4-dione (**9a**) and triethyl orthoformate in a yield of 29.3%. C$_{14}$H$_{12}$N$_4$O$_2$; mp: 258 °C (DMF); ^{1}H NMR (600 MHz, DMSO-d_6) δ_H: 8.16–8.12 (m, 1H), 7.53–7.50 (m, 2H), 7.50–7.48 (m, 2H), 7.48–7.45 (m, 1H), 3.52–3.50 (s, 3H), 3.28–3.26 (s, 3H); ^{13}C NMR (150 MHz, DMSO-d_6) δ_C: 155.00 (2 × C), 151.80 (CH), 150.10 (C), 148.90 (C), 142.00 (2 × C), 130.10 (CH), 129.25 (2 × CH), 127.00 (2 × CH), 30.10 (CH$_3$), 28.20 (CH$_3$); MS (EI, 70 EV) m/z: 268 (M$^+$); IR (KBr) ν_{max}: 3165, 1697, 1659, 1561, 1525, 1472, 1356, 1298, 1229, 1060, 786, 758, 746, 707 cm^{-1}; Anal. Calcd for C$_{14}$H$_{12}$N$_4$O$_2$: C, 62.68; H, 4.51; N, 20.88. Found: C, 62.00; H, 4.70; N, 20.30.

5.2.6. 6-(3-Chlorophenyl)-1,3-dimethyl-1*H*-pteridine-2,4-dione (10b)

Compound **10b** was prepared from 6-amino-5-{[1-(3-chlorophenyl)-meth-(*E*)-ylidene]-amino}-1,3-dimethyl-1*H*-pyridine-2,4-dione (**9b**) and triethyl orthoformate in a yield of 27.1%. C$_{14}$H$_{11}$ClN$_4$O$_2$; mp: 233–236 °C (DMF); ^{1}H NMR (600 MHz, CDCl$_3$) δ_H: 9.06–9.04 (s, 1H), 8.11–8.09 (s, 1H), 7.99–7.95 (m, 1H), 7.48–7.45 (m, 2H), 3.79–3.72 (s, 3H), 3.60–3.55 (s, 3H); ^{13}C NMR (150 MHz, CDCl$_3$) δ_C: 160.00 (C), 150.02 (C), 147.00 (C, CH), 144.90 (C), 136.30 (C), 135.10 (C), 130.02 (CH), 130.00 (CH), 127.00 (CH), 126.80 (CH), 125.00 (C), 29.22 (CH$_3$), 29.00 (CH$_3$); MS (EI, 70 eV) m/z: 302 (M$^+$); IR (KBr) ν_{max}: 3066, 1717, 1669, 1545, 1505, 1424, 1336, 1218, 1105, 1010, 908, 794, 750, 739, 687 cm^{-1}; Anal. Calcd for C$_{14}$H$_{11}$ClN$_4$O$_2$: C, 55.55; H, 3.66; N, 18.51. Found: C, 56.20; H, 3.60; N, 18.60.

5.2.7. 6-[(*E*)-2-(3-Chlorostyryl)]-1,3-dimethyl-1*H*-pteridine-2,4-dione (10d)

Compound **10d** was prepared from 6-amino-5-[(*E*)-3-(3-chlorophenyl)-prop-2-en-(*E*)-ylideneamino]-1,3-dimethyl-1*H*-pyrimidine-2,4-dione (**9d**) and triethyl orthoformate in a yield of 7.2%. C$_{16}$H$_{13}$ClN$_4$O$_2$; mp: 270 °C (acetone); ^{1}H NMR (600 MHz, CDCl$_3$) δ_H: 8.65 (s, 1H), 7.65 (d, 1H, J = 15.97 Hz), 7.61–7.36 (m, 4H), 7.27 (d, 1H, J = 15.29 Hz), 3.70 (s, 3H), 3.50 (s, 3H); ^{13}C NMR (150 MHz, CDCl$_3$) δ_C: 159.06 (C), 149.68 (C), 146.43 (CH), 145.14 (C), 138.23 (C), 135.57 (C), 133.78 (C), 129.84 (2 × CH), 127.51 (2 × CH), 125.63 (C), 123.49 (CH), 122.24 (CH), 29.06 (CH$_3$), 27.00 (CH$_3$); MS (EI, 70 eV) m/z: 328 (M$^+$); IR (KBr) ν_{max}: 3096, 3062, 2954, 1719, 1670, 1539, 1501, 1460, 1346, 1287, 1220, 1010, 889, 794, 750, 727, 681 cm^{-1}; Anal. Calcd for C$_{16}$H$_{13}$ClN$_4$O$_2$: C, 58.46; H, 3.99; N, 17.04. Found: C, 59.80; H, 4.10; N, 16.70.

5.3. Biological evaluation

Approval for this study was obtained from the Ethics Committee for Research on Experimental Animals of the North-West University (Potchefstroom Campus).

5.3.1. MAO-B inhibition study

Mitochondria from baboon liver tissue were isolated as follows:[43] Baboon liver tissue (200 g) was grinded through a Foley mill and homogenised with a glass/teflon homogeniser in 356 mL potassium phosphate buffer (10 mM, pH 7–7.2) containing sucrose (0.25 M) and ethylenediaminetetra-acetic acid (EDTA) (0.5 mM). The homogenate was diluted to 620 mL with the above solution and centrifuged at 600g for 15 min. The supernatant was decanted through a cheese cloth and again centrifuged at 10,400g for 15 min. The pellet obtained was homogenised in a small volume of a potassium phosphate buffer (10 mM, pH 7–7.2) containing sucrose (0.25 M) and diluted to a final volume of 124 mL with the same buffer. The homogenate was centrifuged at 7500g for 15 min and the resulting pellet was homogenised in a small volume of a buffer containing tris (10 mM, pH 7–7.2) and potassium chloride (0.15 M). The homogenate was diluted to a final volume of 52 mL, centrifuged at 7500g for 15 min and the pellet obtained was stored at −70 °C in 300 µL aliquots. Before use, the mitochondrial isolate was suspended in 300 µL of sodium phosphate buffer (100 mM, pH 7.4) containing glycerol (50%, w/v) and the protein concentration was determined by the Bradford method[44] using bovine serum albumin as reference standard. As noted earlier, the mitochondrial fraction obtained from baboon liver tissue is devoid of MAO-A activity[27] and therefore inactivation of the enzyme with clorgyline was unnecessary. The MAO-A and -B mixed substrate MMTP (K_m = 60.9 µM for baboon liver MAO-B)[25] was used as substrate for the inhibition studies. All incubations were performed in sodium phosphate buffer (100 mM, pH 7.4) and contained MMTP (50 µM), the mitochondrial isolate (0.15 mg protein/mL), and various concentrations of the test inhibitors, producing a final incubation volume of 500 µL. Stock solutions of the test inhibitors were prepared in DMSO and added to the incubation mixtures to yield a final DMSO concentration of 4% (v/v). DMSO concentrations higher than 4% are reported to inhibit MAO-B.[45] Samples were incubated at 37 °C for 10 min, a time period for which dihydropyridinium metabolite formation is reported to be linear.[27] The enzyme reactions were terminated by the addition of 10 µL perchloric acid (70%) and centrifuged at 16,000g for 10 min. The supernatant fractions were removed and the concentrations of the MAO-B generated product, MMDP$^+$, were measured spectrophotometrically at 420 nm using a Shimadzu® MultiSpec-1501 spectrophotometer (ε = 25,000 M^{-1}). The IC$_{50}$ values were determined from plots of the rate of MAO-B catalysed MMDP$^+$ formation versus the logarithm of the inhibitor concentration. For this purpose the Prism® 4.02 (GraphPad, Sorrento Valley, CA) software package was employed. At least eight different concentrations of the test inhibitor, spanning 3 orders of magnitude were used to construct the sigmoidal dose–response curve. The IC$_{50}$ values are reported as mean ± standard error of the mean (SEM) of duplicate determinations.

5.3.2. NOS inhibition study

Brain tissue (1 g/5 mL) of male Sprague-Dawley rats were homogenised in a solution consisting of 4-(2-hydroxyethyl)piperazine-1-ethanesulfonic acid (HEPES) (100 mM, pH 7.4), sucrose (320 mM), EDTA (1 mM), D/L-dithiothretiol (1 mM), leupeptin (10 µg/mL), soybean-trypsin inhibitor (10 µg/mL) and aprotinin (2 µg/mL).

After 10 s of homogenation at 4 °C phenylmethylsulfonyl fluoride (PMSF) (10 µM/mL) was added and the mixture was homogenised for an additional 30 s. Thereafter the homogenate was centrifuged at 12,000g for 10 min. The supernatant was collected and divided into 2 mL aliquots, which were assayed immediately or snap frozen and stored at −70 °C.

Haemoglobin was converted to its oxygenated form as follows: Crystallised haemoglobin (25 mg) was dissolved in 1 mL cold HEPES buffer[46] and reduced with an excess sodium dithionate (0.958 mg). Oxygen was blown over the surface and the solution gently swirled for 15 min. The gradual colour change from dark red to bright red was indicative of the oxygenation of haemoglobin.

Purification and desalting of the resulting oxyHb solution was performed using a Sephadex® G-25 column.

The test compounds were dissolved in DMSO to yield a concentration of 5% DMSO in the final incubation mixtures. The incubations contained HEPES (500 µM), test inhibitor, CaCl$_2$ (250 µM) and tissue homogenate (2.36 mg of the original brain tissue) and were pre-incubated for 3 min at 37 °C before the reaction was started by the addition of oxyHb (~1.09 µM), NADPH (100 µM) and L-arginine (100 µM). UV–vis scans (1 scan every 10 s) were recorded between 390 and 430 nm for a period of 10 min. The metHb production was estimated by subtracting the absorbance at 411 nm from the absorbance at 401 nm. The IC$_{50}$ values for the inhibition of NOS were determined from plots of the rate of metHb formation versus the logarithm of the inhibitor concentration. For this purpose Prism® 4.02 was used.

5.4. Molecular modeling

All computational studies were carried out with Discovery Studio® 1.7 (Accelrys Software Inc., San Diego, CA). The crystal structure of human MAO-B (PDB code: 2V5Z)[32] recovered from the Brookhaven Protein Database (www.rcsb.org/pdb) was applied as receptor model for the docking procedure. Manipulation of the crystal structure followed wherein the valences of the co-crystallised ligand (safinamide) and FAD cofactor were corrected and hydrogen atoms added. The receptor protein was then typed by applying the CHARMm forcefield before performing a three-step minimisation protocol (steepest descent, conjugate gradient and adopted basis Newton–Rapheson), wherein the protein backbone was kept rigid and the Generalised Born with Simple Switching implicit solvation model was used to account for the effects of the aqueous environment. Minimisation of the receptor protein was considered necessary since the protein X-ray structure might contain residual energetic tensions from the crystallisation process. The safinamide (in the A chain) was subsequently eliminated from the energy-minimised receptor protein and the backbone constraint was removed, where after it was used as the starting model for the docking simulation. The ligands to be docked were first constructed within DS Visualizer Pro® and then prepared for the docking simulations employing the Prepare Ligands application of Discovery Studio® 1.7. The structures were docked into the receptor model with the LigandFit application, which applied total ligand flexibility whereby the final ligand conformations were determined by the Monte Carlo conformation search method set to a variable number of trial runs. The docked ligand conformations were further refined using in situ ligand minimisation with the Smart Minimizer algorithm. The best solution for each docked ligand was adjudged by the DockScore scoring function of LigandFit. All the application modules within Discovery Studio® 1.7 were set to their default values and 10 docking solutions were allowed for each ligand.

Acknowledgement

References and notes

1. Van der Schyf, C. J.; Geldenhuys, W. J.; Youdim, M. B. H. *J. Neurochem.* **2006**, *99*, 1033.
2. Jellinger, K. A. *J. Neural Transm.* **2003**, *65*, 101.
3. Smid, P.; Coolen, H. K. A. C.; Keizer, H. G.; Van Hes, R.; De Moes, J.-P.; Den Hartog, A. P.; Stork, B.; Plekkenpol, R. H.; Niemann, L. C.; Stroomer, C. N. J.; Tulp, M. T. M.; Van Stuivenberg, H. H.; McCreary, A. C.; Hesselink, M. B.; Herremans, A. H. J.; Kruse, C. G. *J. Med. Chem.* **2005**, *48*, 6855.
4. Saura, J.; Bleuel, Z.; Ulrich, J.; Mendelowitsch, A.; Chen, K.; Shih, J. C.; Malherbe, P.; Da Prada, M.; Richards, J. G. *Neuroscience* **1996**, *70*, 755.
5. Fowler, C. J.; Wiberg, A.; Oreland, L.; Marcusson, J.; Winblad, B. *J. Neural Transm. (Gen. Sect.)* **1980**, *49*, 1.
6. Maimone, D.; Dominici, R.; Grimaldi, L. M. E. *Eur. J. Pharmacol.* **2001**, *413*, 11.
7. Saura, J.; Luque, J. M.; Cesura, A. M.; Da Prada, M.; Chan-Palay, V.; Huber, G.; Loffler, J.; Richards, J. G. *Neuroscience* **1994**, *62*, 15.
8. Palmer, R. M. J.; Ferrige, A. G.; Moncada, S. *Nature* **1987**, *327*, 524.
9. Moncada, S.; Palmer, R. M. J.; Higgs, E. A. *Biochem. Pharmacol.* **1989**, *38*, 1709.
10. Hibbs, J. B., Jr.; Vavrin, Z.; Taintor, R. R. *J. Immunol.* **1987**, *138*, 550.
11. Garthwaite, J. In *Nitric Oxide from l-Arginine: A Bioregulatory System*; Moncada, S., Higgs, E. A., Eds.; Elsevier: Amsterdam, 1990; pp 115–137.
12. Burnett, A. L.; Lowenstein, C. J.; Bredt, D. S.; Chang, T. S. K.; Snyder, S. H. *Science* **1992**, *257*, 401.
13. Cheshire, D. R. *IDrugs* **2001**, *4*, 795.
14. Endres, M.; Laufs, U.; Liao, J. K.; Moskowitz, M. A. *Trends Neurosci.* **2004**, *27*, 283.
15. Togo, T.; Katsuse, O.; Iseki, E. *Neurol. Res.* **2004**, *26*, 563.
16. Dawson, V.; Dawson, T.; Bartley, D.; Uhl, G.; Snyder, S. *J. Neurosci.* **1993**, *13*, 2651.
17. Dawson, V. L.; Dawson, T. M. *J. Chem. Neuroanat.* **1996**, *10*, 179.
18. Chen, J.-F.; Xu, K.; Petzer, J. P.; Staal, R.; Xu, Y.-H.; Beilstein, M.; Sonsalla, P. K.; Castagnoli, K.; Castagnoli, N., Jr.; Schwarzschild, M. A. *J. Neurosci.* **2001**, *21*, 143.
19. Petzer, J. P.; Steyn, S.; Castagnoli, K. P.; Chen, J.-F.; Schwarzschild, M. A.; Van der Schyf, C. J.; Castagnoli, N., Jr. *Bioorg. Med. Chem.* **2003**, *11*, 1299.
20. Chen, J.-F.; Steyn, S.; Staal, R.; Petzer, J. P.; Xu, K.; Van der Schyf, C. J.; Castagnoli, K.; Sonsalla, P. K.; Castagnoli, N., Jr.; Schwarzschild, M. A. *J. Biol. Chem.* **2002**, *277*, 36040.
21. Vlok, N.; Malan, S. F.; Castagnoli, N., Jr.; Bergh, J. J.; Petzer, J. P. *Bioorg. Med. Chem.* **2006**, *14*, 3512.
22. Crane, B. R.; Arvai, A. S.; Ghosh, D. K.; Wu, C.; Getzoff, E. D.; Stuehr, D. J.; Tainer, J. A. *Science* **1998**, *279*, 2121.
23. Raman, C. S.; Li, H.; Martásek, P.; Král, V.; Masters, B. S. S.; Poulos, T. L. *Cell* **1998**, *95*, 939.
24. Mayer, B.; Werner, E. R. *Naunyn-Schmiedeberg's Arch. Pharmacol.* **1995**, *351*, 453.
25. Werner, E. R.; Pitters, E.; Schmidt, K.; Wachter, H.; Werner-Felmayer, G.; Mayer, B. *Biochem. J.* **1996**, *320*, 193.
26. Yoneda, F.; Higuchi, M. *J. Chem. Soc., Perkin Trans. 1* **1977**, *11*, 1336.
27. Inoue, H.; Castagnoli, K.; Van der Schyf, C.; Mabic, S.; Igarashi, K.; Castagnoli, N., Jr. *J. Pharmacol. Exp. Ther.* **1999**, *291*, 856.
28. Cheng, Y. C.; Prusoff, W. H. *Biochem. Pharmacol.* **1973**, *22*, 3099.
29. Salter, M.; Knowles, R. G. In *Nitric Oxide Protocols*; Titheradge, M. A., Ed.; Humana Press: Totowa, NJ, 1998; pp 61–65.
30. Salter, M.; Knowles, R. G.; Moncada, S. *FEBS Lett.* **1991**, *291*, 145.
31. Joubert, J.; Van Dyk, S.; Malan, S. F. *Bioorg. Med. Chem.* **2008**, *16*, 8952.
32. Binda, C.; Wang, J.; Pisani, L.; Caccia, C.; Carotti, A.; Salvati, P.; Edmondson, D. E.; Mattevi, A. *J. Med. Chem.* **2007**, *50*, 5848.
33. Binda, C.; Li, M.; Hubálek, F.; Restelli, N.; Edmondson, D. E.; Mattevi, A. *Proc. Natl. Acad. Sci. U.S.A.* **2003**, *100*, 9750.
34. Boström, J.; Greenwood, J. R.; Gottfries, J. *J. Mol. Graphics Modell.* **2003**, *21*, 449.
35. Pretorius, J.; Malan, S. F.; Castagnoli, N., Jr.; Bergh, J. J.; Petzer, J. P. *Bioorg. Med. Chem.* **2008**, *16*, 8676.
36. Morphy, R.; Rankovic, Z. *J. Med. Chem.* **2005**, *48*, 6523.
37. Youdim, M. B. H.; Buccafusco, J. J. *J. Neural Transm.* **2005**, *112*, 519.
38. Van den Berg, D.; Zoellner, K. R.; Ogunrombi, M. O.; Malan, S. F.; Terre'Blanche, G., ; Castagnoli, N., Jr.; Bergh, J. J.; Petzer, J. P. *Bioorg. Med. Chem.* **2007**, *15*, 3692.
39. Pitts, S. M.; Markey, S. P.; Murphy, D. L.; Weisz, A. In *MPTP: A Neurotoxin Producing a Parkinsonian Syndrome*; Markey, S. P., Castagnoli, N., Jr., Trevor, A. J., Kopin, I. J., Eds.; Academic Press: New York, 1986; pp 703–716.
40. Blicke, F. F.; Godt, H. C. *J. Am. Chem. Soc.* **1954**, *76*, 2798.
41. Baker, B. R.; Janson, E. E.; Vermeulen, N. M. J. *J. Med. Chem.* **1969**, *12*, 898.
42. Bissel, P.; Bigley, M. C.; Castagnoli, K.; Castagnoli, N., Jr. *Bioorg. Med. Chem.* **2002**, *10*, 3031.
43. Salach, J. I.; Weyler, W. *Methods Enzymol.* **1987**, *142*, 627.
44. Bradford, M. M. *Anal. Biochem.* **1976**, *72*, 248.
45. Gnerre, C.; Catto, M.; Leonetti, F.; Weber, P.; Carrupt, P.-A.; Altomare, C.; Carotti, A.; Testa, B. *J. Med. Chem.* **2000**, *43*, 4747.
46. Corbett, J. A.; McDaniel, M. L. *Methods* **1996**, *10*, 21.